

Escape from Cells: Deep Kd-Networks for The Recognition of 3D Point Cloud Models

Roman Klokov

Skolkovo Institute of Science and Technology

roman.klokov@skoltech.ru

Victor Lempitsky

Skolkovo Institute of Science and Technology

lempitsky@skoltech.ru

Abstract

We present a new deep learning architecture (called *Kd-network*) that is designed for 3D model recognition tasks and works with unstructured point clouds. The new architecture performs multiplicative transformations and share parameters of these transformations according to the subdivisions of the point clouds imposed onto them by *Kd-trees*. Unlike the currently dominant convolutional architectures that usually require rasterization on uniform two-dimensional or three-dimensional grids, *Kd-networks* do not rely on such grids in any way and therefore avoid poor scaling behaviour. In a series of experiments with popular shape recognition benchmarks, *Kd-networks* demonstrate competitive performance in a number of shape recognition tasks such as shape classification, shape retrieval and shape part segmentation.

1. Introduction

As the 3D world around us is getting scanned and digitized and as the archives of human-designed models are growing in size, recognition and analysis of 3D geometric models are gaining importance. Meanwhile, deep convolutional networks (ConvNets) [15] have excelled at solving analogous recognition tasks for 2D image datasets. It is therefore natural that a lot of research currently aims at the adaptation of deep ConvNets to 3D models [35, 18, 4, 34, 33, 21, 30, 2, 3].

Such adaptation is non-trivial. Indeed, the most straightforward way to make ConvNets applicable to 3D data, is to rasterize 3D models onto uniform voxel grids. Such approach however leads to excessively large memory footprints and slow processing times. Consequently, works that follow this path [35, 18, 4, 34, 33, 16] use small spatial resolutions (e.g. $64 \times 64 \times 64$), which clearly lag behind grid resolutions typical for processing 2D data, and is likely to be insufficient for the recognition tasks that require attention to fine details in the models.

To solve this problem, we take inspiration from the long history of research in computer graphics and computational geometry communities [25, 10], where a large number of indexing structures that are far more scalable than uniform grids have been proposed, including *kd-trees* [1], *octrees* [19], binary spatial partition trees [28], *R-trees* [11], constructive solid geometry [23], etc. Our work was motivated by the question, whether at least *some of these indexing structures are amenable for forming the base for deep architectures*, in the same way as uniform grids form the base for the computations, data alignment and parameter sharing inside convolutional networks.

In this work, we pick one of the most common 3D indexing structures (a *kd-tree* [1]) and design a deep architecture (a *Kd-network*) that in many respects mimics ConvNets but uses the *kd-tree* structure to form the computational graph, to share the learnable parameters, and to compute a sequence of hierarchical representations in a feed-forward bottom-up fashion. In a series of the experiments, we show that *Kd-networks* come close (or even exceed) ConvNets in terms of accuracy for recognition operations such as classification, retrieval and part segmentation. At the same time, *Kd-networks* come with smaller memory footprints and more efficient computations at train and at test time thanks to the improved ability of *Kd-trees* to index and structure 3D data as compared to uniform voxel grids.

Below, we first review the related work on convolutional networks for 3D models in Section 2. We then discuss the *Kd-network* architecture in Section 3. An extensive evaluation on toy data (a variation of MNIST) and standard benchmarks (ModelNet10, ModelNet40, SHREC’16, ShapeNet part datasets) is presented in Section 4. We summarize the work in Section 5.

2. Related Work

Several groups investigated application of ConvNets to the rasterizations of 3D models on uniform 3D grids [35, 18]. The improvements include combinations of generative and very deep discriminative architectures [4, 34]. De-

spite considerable success in coarse-level classification, the reliance on uniform 3D grids for data representation makes scaling of such approaches to fine-grained tasks and high spatial representations problematic. To improve the scalability [33, 16] have considered sparse ways to define convolutions, while still using uniform 3D grids for representations.

Another approach [30, 21] is to avoid the use of 3D grids, and instead apply two-dimensional ConvNets to 2D projections of 3D objects, while pooling representations corresponding to different views. Despite gains in efficiency, such approach may not be optimal for hard 3D shape recognition tasks due to the loss of information associated with the projection operation. A group of approaches (such as spectral ConvNets [6, 2] and anisotropic ConvNets [3]) generalize ConvNets to non-Euclidean geometries, such as mesh surfaces. This group of approaches requires and utilizes mesh topology (not needed for Kd-networks). This have shown very good performance for local correspondence/matching tasks, though their performance on standard shape recognition and retrieval benchmarks has not been reported. Kd-networks as well as the PointNet architecture [20] work directly with points and therefore can take the representations computed with intrinsic ConvNets as inputs. Such configuration is likely to combine at least some of the advantages of extrinsic and intrinsic ConvNets, but its investigation is left for future work.

Aside from their connections to convolutional networks that we discuss in detail below, Kd-networks are related to recursive neural networks [29]. Both recursive neural networks and Kd-networks have tree-structured computational graphs. However, the former share parameters across all nodes in the computational tree graph, while sharing of parameters in Kd-networks is more structured, which allows them to achieve competitive performance.

3. Shape Recognition with Kd-Networks

We now introduce Kd-networks, starting with the discussion of their input format (Kd-trees of certain size), then discussing the bottom-up computation of representations performed by Kd-networks, and finally discussing supervised parameter learning.

Input. The new deep architecture (the Kd-network) works with Kd-trees constructed for 3D point clouds. Kd-networks can also consider and utilize properties of individual input points (such as color, reflectivity, normal direction) if they are known. At train time, Kd-network works with point clouds of a fixed size $N = 2^D$ (point clouds of different sizes can be reduced to this size using sub- or oversampling). A Kd-tree is constructed recursively in a top-down fashion by picking the coordinate axis with the largest range (span) of point coordinates, and splitting the set of points into two equally-sized subsets, subsequently

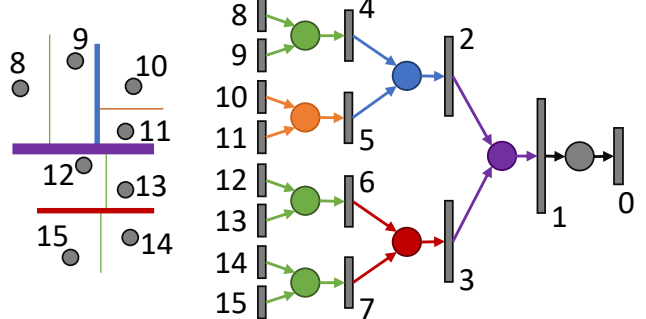


Figure 1. A Kd-tree built on the point cloud of eight points (left), and the associated Kd-network built for classification (right). We number nodes in the Kd-tree from the root to leaves. Therefore leaf nodes, which correspond to original points, are numbered starting from 8. The arrows indicate information flow during forward pass (inference). The leftmost bars correspond to leaf (point) representations. The rightmost bar corresponds to inferred class posteriors v_0 . Circles correspond to linear (affine) transformations with learnable parameters. Colors of the circles indicate parameter sharing, as splits of the same type (same orientation, same tree level – three “green” splits in this example) share the transformation parameters.

recurring to each of them. As a result, a balanced Kd-tree \mathcal{T} of depth D is produced that contains $N-1 = 2^D-1$ non-leaf nodes.

Each non-leaf node $V_i \in \mathcal{T}$ is thus associated with one of three splitting directions d_i (along x , y or z -axis, i.e. $d_i \in \{x, y, z\}$) and a certain split position (threshold) τ_i . A tree node is also characterized by the level $l_i \in \{1, \dots, D-1\}$, with $l_i=1$ for the root node, and $l_i=D$ for tree leaves that contain individual 3D points. We assume that the nodes in the balanced tree are numbered in the standard top-down fashion, with the root being the first node, and with the i th node having children with numbers $c_1(i) = 2i$ and $c_2(i) = 2i + 1$.

Processing data with Kd-networks. Given an input Kd-tree \mathcal{T} , a pretrained Kd-network computes vectorial representations v_i associated with each node of the tree. For the leaf nodes, these representations are given as k -dimensional vectors describing the individual points, associated with those leaves. The representations corresponding to non-leaf nodes are computed in the bottom-up fashion (Figure 1). Consider, a non-leaf node i at the level $l(i)$ with children $c_1(i)$ and $c_2(i)$ at the level $l(i) + 1$, for which the representations $v_{c_1(i)}$ and $v_{c_2(i)}$ have already been computed. Then, the vector representation v_i is computed as follows:

$$v_i = \begin{cases} \phi(W_x^{l_i}[v_{c_1(i)}; v_{c_2(i)}] + b_x^{l_i}), & \text{if } d_i = x, \\ \phi(W_y^{l_i}[v_{c_1(i)}; v_{c_2(i)}] + b_y^{l_i}), & \text{if } d_i = y, \\ \phi(W_z^{l_i}[v_{c_1(i)}; v_{c_2(i)}] + b_z^{l_i}), & \text{if } d_i = z, \end{cases} \quad (1)$$

or in short form:

$$\mathbf{v}_i = \phi(W_{d_i}^{l_i} [\mathbf{v}_{c_1(i)}; \mathbf{v}_{c_2(i)}] + \mathbf{b}_{d_i}^{l_i}). \quad (2)$$

Here, $\phi(\cdot)$ is some non-linearity (e.g. REctified Linear Unit $\phi(a) = \max(a, 0)$), and square brackets denote concatenation. The linear (affine) transformation in (1) is defined by the learnable parameters $\{W_x^{l_i}, W_y^{l_i}, W_z^{l_i}, \mathbf{b}_x^{l_i}, \mathbf{b}_y^{l_i}, \mathbf{b}_z^{l_i}\}$ of the layer l_i . Thus, depending on the splitting direction d_i of the node, one of the three affine transforms followed by a simple non-linearity is applied.

The dimensionality of the matrices and the bias vectors are determined by the dimensionalities m^1, m^2, \dots, m^D of representations at each level of the tree. The W_x^l, W_y^l , and W_z^l matrices at the l th level thus have the dimensionality $m^l \times 2m^{l+1}$ (recall that the levels are numbered from the root to the leaves) and the bias vectors $\mathbf{b}_x^l, \mathbf{b}_y^l, \mathbf{b}_z^l$ have the dimensionality m^l .

Once the transforms (1) are applied in a bottom-up order, the root representation $\mathbf{v}_1(\mathcal{T})$ for the sample \mathcal{T} is obtained. Naturally, it can be passed through several additional linear and non-linear transformations (“fully-connected layers”). In our classification experiments, we directly learn linear classifiers using $\mathbf{v}_1(\mathcal{T})$ representation as an input. In this case, the classification network output the vector of unnormalized class odds:

$$\mathbf{v}_0(\mathcal{T}) = W^0 \mathbf{v}_1(\mathcal{T}) + \mathbf{b}^0, \quad (3)$$

where W^0 and \mathbf{b}^0 are the parameters of the final linear multi-class classifier.

Learning to classify. A Kd-network is a feed-forward neural network that has the learnable parameters $\{W_x^j, W_y^j, W_z^j, \mathbf{b}_x^j, \mathbf{b}_y^j, \mathbf{b}_z^j\}$ at each of the $D-1$ non-leaf levels $j \in \{1..D-1\}$, as well as the learnable parameters $\{W^0, \mathbf{b}^0\}$ for the final classifier. Standard backpropagation method can be used to compute the gradient of the loss function w.r.t. network parameters. The network parameters can thus be learned from the dataset of labeled Kd-trees using standard stochastic optimization algorithms and standard losses, such as cross-entropy on the network output $\mathbf{v}_0(\mathcal{T})$ (3).

Learning to retrieve. It is straightforward to learn the representation (3) to produce not the class odds, but a descriptor vector of a certain dimensionality that characterizes the shape and can be used for retrieval. The parameters of the Kd-network can then be learned using backpropagation using any of the embedding-learning losses that observe examples of matching (e.g. same-class) and non-matching (e.g. different-class) shapes. In our experiments, we use a recently proposed histogram loss [32], but more traditional losses such as Siamese loss [5, 8] or triplet loss [27] could be used as well.

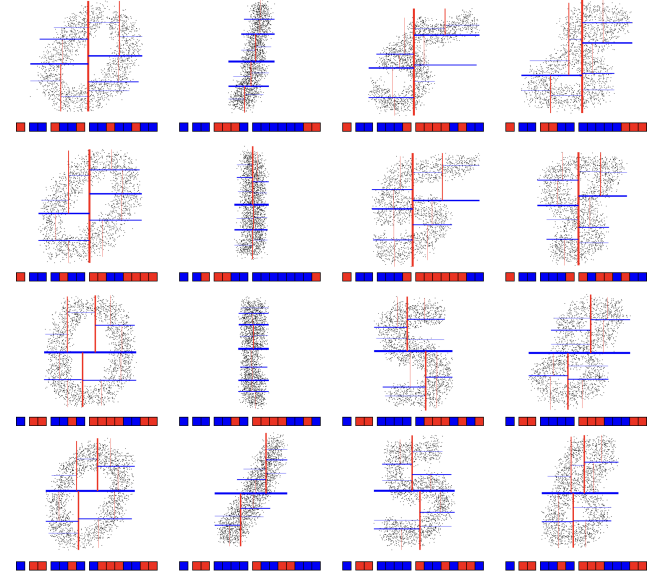


Figure 2. Kd-trees for MNIST clouds. We visualize several examples of 2D point clouds for MNIST (see text for description) with constructed Kd-trees. The type of split is encoded with color and for each example the types of splits for the first four levels of the tree are shown below. Importantly, the structure of the Kd-tree serves as a shape descriptor (e.g. ‘ones’ are dominated by vertical splits, and ‘zeroes’ tend to interleave vertical and horizontal splits as a kd-tree is traversed from the root to a leaf).

3.1. Properties of Kd-networks

Here we discuss the properties of the Kd-networks and also relate them to some of the properties of ConvNets.

Layerwise parameter sharing. Similarly to ConvNets, Kd-networks process the inputs by applying a sequence of parallel spatially-localized multiplicative operations interleaved with non-linearities. Importantly, just as ConvNets share their multiplicative parameters for localized multiplications (convolution kernels) across different spatial locations, Kd-networks also share the multiplicative parameters $\{W_x^j, W_y^j, W_z^j, \mathbf{b}_x^j, \mathbf{b}_y^j, \mathbf{b}_z^j\}$ across all nodes at the tree level j .

Hierarchical representations. ConvNets apply bottom-up processing and compute a sequence of representations that correspond to progressively large parts of images. The procedure is hierarchical, in the sense that a representation of a spatial location at a certain layer is obtained from the representations of multiple surrounding locations at the preceding layer using linear and non-linear operations. All this is mimicked in Kd-networks, the only difference being that the receptive fields of two different nodes at the same level of the kd-tree are non-overlapping.

Partial invariance to jitter. Convolutional networks that use pooling operations and/or strides larger than one are known to possess partial invariance to small spatial jit-

ter in the input. Kd-networks are also invariant to such jitter (unless such jitter strongly perturbs the representations of leaf nodes). This is because the key forward-propagation operation (1) does ignore splitting thresholds τ_i . Thus, any small spatial perturbation of input points that leave the topology of the Kd-tree intact can only affect the output of a Kd-network via the leaf representations (which as will be revealed in the experiments play only secondary role in kd-networks).

Non-invariance to rotations. Similarly to ConvNets, Kd-networks are not invariant to rotations, as the underlying Kd-trees are not invariant to them. In this aspect, Kd-networks are inferior to implicit ConvNets [6, 2, 3]. Standard tricks to handle variable orientations include pre-alignment (using heuristics or network branches that predicts geometric transforms of the data [13, 20]) as well as pooling over augmentations [14] (or simply training with excessive augmentations).

Role of Kd-tree structure. The role of the underlying Kd-trees in the process of Kd-network data processing is two-fold. Firstly, the underlying Kd-tree determines which leaf representations are getting combined/merged together and in which order. Secondly, the structure of the underlying Kd-tree can be regarded as a shape descriptor itself (Figure 2) and thus serves the source of the information irrespective of what the leaf representations are. The Kd-network then serves as a mechanism for extracting the shape information contained in the Kd-tree structure. As will be revealed in the experiments, the second aspect is of considerable importance, as even in the absence of the meaningful leaf representations, Kd-networks are able to recognize shapes well solely based on the Kd-tree structure.

3.2. Extension for segmentation

Kd-network architecture can be extended to perform semantic/part segmentation tasks in the same way as ConvNets. In this work, we mimic the encoder-decoder (hourglass-shaped) architecture with *skip connections* (Figure 3) that has been proposed for ConvNets in [17, 24]. More formally, during inference firstly the representations \mathbf{v}_i are computed using (2), and then the second representation vector $\tilde{\mathbf{v}}_i$ is computed at each node i . The computations of the second representation proceed by setting $\tilde{\mathbf{v}}_1 = \mathbf{v}_1$ and then using the following chain of top-down computations:

$$[\tilde{\mathbf{v}}_{c_1(i)}; \tilde{\mathbf{v}}_{c_2(i)}] = \phi(\tilde{W}_{d_i}^{l_i} \tilde{\mathbf{v}}_i + \tilde{\mathbf{b}}_{d_i}^{l_i} + [S^{l_i} \mathbf{v}_{c_1(i)} + \mathbf{t}^{l_i}; S^{l_i} \mathbf{v}_{c_2(i)} + \mathbf{t}^{l_i}]), \quad (4)$$

where $\tilde{W}_{d_i}^{l_i}$ and $\tilde{\mathbf{b}}_{d_i}^{l_i}$ are the parameters of the affine transformation that map the parent’s representation to the children representations stacked on top of each other, while S^{l_i} and \mathbf{t}^{l_i} are the parameters of the affine transformation within the skip connection from $\mathbf{v}_{c_1(i)}$ to $\tilde{\mathbf{v}}_{c_1(i)}$ (as well as from $\mathbf{v}_{c_2(i)}$

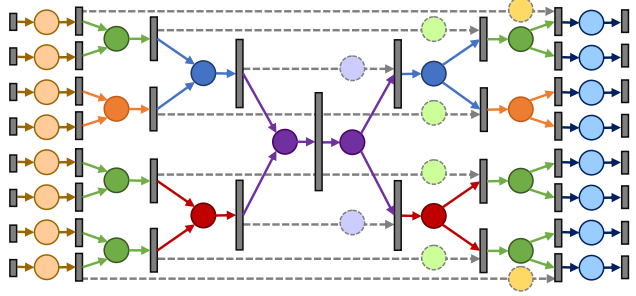


Figure 3. The architecture for parts segmentation (individual point classification) for the point cloud shown in Figure 1 (left). Arrows indicate computations that transform the representations (bars) of different nodes. Circles correspond to affine transforms followed by non-linearities. Similarly colored circles on top of each other share parameters. Dashed lines correspond to skip-connections (some “yellow” skip connections are not shown for clarity). The input representations are processed by an additional transform (light-brown) and there are additional transforms applied to every leaf representation independently at the end of the architecture (light-blue).

to $\tilde{\mathbf{v}}_{c_2(i)}$). In our implementation, the former set of parameters depends on split orientation, while the latter depends on the node depth only.

Once the computations (4) produce the representations $\tilde{\mathbf{v}}_i$ for leaf nodes, we further compute the part class probabilities (odds) using several fully-connected layers interleaved with ReLU non-linearities. In the experiments, we maintain the same dimensionality of \mathbf{v}_i and $\tilde{\mathbf{v}}_i$ (thus, the skip-connection matrices S^{l_i} are square-shaped). We insert an additional layer (affine and ReLU) prior to the input of the architecture described above (in order to make both \mathbf{v}_i and $\tilde{\mathbf{v}}_i$ high-dimensional). All parameters of fully-connected layers mentioned in this paragraph are shared across all leafs.

3.3. Implementation details

Leaf representation. As mentioned above, for a leaf node i a representation \mathbf{v}_i can be defined in several ways. In our experiments, unless stated otherwise, we use normalized 3D coordinates obtained by putting the center of mass of the shape at origin and rescaling the input point cloud to fit the $[-1; 1]^3$ 3D box.

Data augmentation. Similarly to other machine learning architectures, the performance of Kd-networks can be improved through training data augmentations. Below, we experiment with applying perturbing geometric transformations to 3D point clouds. Additionally, we found the injecting randomness into Kd-tree construction very useful. For that, we randomize the choice of split directions using the

	ModelNet10	ModelNet40
MVCNN [30]	-	90.1
FusionNet [12]	93.1	90.8
VRN Single [4]	93.6	91.3
PointNet [20]	-	89.2
Set-conv [22]	-	90.0
Kd-network (depth 10)	93.3	90.6
Kd-network (depth 15)	94.0	91.8
VRN Ensemble [4]	97.1	95.5

Table 1. **Classification results on ModelNet benchmarks.** Comparison of accuracies of Kd-networks (depth 10 and 15) with state-of-the-art. Kd-networks outperform all single model architectures, while performing worse than VRN ensembles.

following probabilities:

$$P(d_i = j | \hat{r}_i) = \frac{\exp \gamma \hat{r}_i^j}{\sum_{j=x,y,z} \exp \gamma \hat{r}_i^j}, \quad (5)$$

where \hat{r}_i is a vector of ranges normalized to unit sum.

4. Experiments

We now discuss the results of application of Kd-networks to shape classification, shape retrieval and part segmentation tasks benchmarks. For classification, we also evaluate several variations and ablations of Kd-networks. Our implementation of Kd-networks uses Theano [31] and Lasagne [9] libraries.

4.1. Shape classification

Datasets and data processing. We evaluate Kd-networks on datasets of 2D (for illustration purposes) as well as 3D point clouds. 2D point clouds were produced from the **MNIST** dataset [15] by turning centers of non-zero pixels into 2D points. A point cloud of a needed size was then sampled from the resulting set of points with a small random noise added to every coordinate of every point in a cloud. Figure 2 shows examples of resulting point clouds.

The 10-class and the 40-class variations of ModelNet [35] (**ModelNet10** and **ModelNet40**) benchmarks, containing 4899 and 12311 models respectively, were used for 3D shape classifications. The two datasets are split into the training set (3991 and 9843 models) and the test set (909 and 2468 models respectively). In this case, 3D point clouds were computed as follows: firstly, a given number of faces were sampled with the probability proportionate to their surface areas. Then, for the sampled face a random point was taken. The whole sampling procedure thus closely approximated uniform sampling of model surfaces.

Training and test procedures. Additionally we preprocess each object by applying a geometric perturbation and/or noise (as discussed below). Either a deterministic or

	MNIST	ModNet10	ModNet40
Split-based linear	82.4	83.4	73.2
Kd-net RT+SA (no leaf)	98.6	92.7	89.8
Kd-net DT	98.9	89.2	85.7
Kd-net RT	99.1	92.8	89.9
Kd-net RT+TA	99.1	92.9	90.1
Kd-net RT+SA	99.1	93.2	90.6
Kd-net RT+SA+TA	99.1	93.3	90.6

Table 2. **Classification accuracy for baselines and different data augmentations.** The resulting accuracies for the baseline model, the ablated model with trivial leaf representations, as well as Kd-networks trained with various data augmentations. DT = deterministic Kd-trees, RT = randomized Kd-trees, TA = translation augmentation, SA = anisotropic scaling augmentation. All networks are depth 10. See text for discussion.

a randomized Kd-tree is constructed and, finally, the resulting point cloud and leaf representations are used to perform forward-backward pass in the Kd-Network. The models are processed in parallel using mini-batches of size 111. At test time, we use the same augmentations as were used during training and we average predicted class probabilities over ten runs.

We experimented with the following augmentations: (i) proportional translations along every axis (*TR*) of up to ± 0.2 in normalized coordinates; proportional anisotropic rescaling over the two horizontal axes (*AS*) by the number sampled from the 0.66 to 1.5 range. More global augmentations like flips or rotations did not improve results. Additionally, we evaluated both deterministic (DT) and randomized (RT) Kd-trees. For our experiments we fixed the parameter γ in (5) to ten.

Benchmarking classification performance. We compare our approach to the state-of-the-art on the ModelNet10 and ModelNet40 benchmarks in Table 1. We give the results obtained with Kd-trees of depth 10 and depth 15. For depth 10, our architecture firstly obtain leaf representation of size 32 from initial points coordinates with a fully connected layer, then a *Kd-network* obtain intermediate representations of sizes: 32 – 64 – 64 – 128 – 128 – 256 – 256 – 512 – 512 – 128. Resulting representation for a point cloud is directly used to obtain class posteriors with a single fully connected layer. For depth 15, the previous architecture has been modified by changing the size of leaf representation to 8 and by updated progression of intermediate representation sizes: 16 – 16 – 32 – 32 – 64 – 64 – 128 – 128 – 256 – 256 – 512 – 512 – 1024 – 1024 – 128.

In both cases, we used translation-based and anisotropic scaling-based augmentations as well as randomized Kd-tree generation at test and at train time. Note that despite the use of random augmentations, a single model (i.e. a single set of model weights) was evaluated for each of the cases (depth 10 and depth 15). Our results are better than all pre-

vious single-model results on these benchmarks, while being worse than the VRN-ensemble that involves 6 models each trained over the course of 6 days on NVidia Titan X. For ModelNet40 our depth-10 model can be trained in 16 hours, and our depth-15 model can be trained in 5 days using an older NVIDIA Titan Black. Furthermore, more than 75% of the time is spent on point cloud sampling and Kd-tree fitting, while the training itself takes less than a quarter of the mentioned times.

It is also interesting to note that the performance of Kd-networks on the MNIST dataset reaches 99.1% (Table 2), which is in the ballpark of the results obtained with ConvNets (without additional tricks).

Ablations and variants. Kd-networks use two sources of information about each object, namely the leaf representations and the direction of the splits. Note, that the split coordinates are not used in the classification. We assess the relative importance of the two sources of the information using two baselines. Firstly, we consider the baseline for both 2D and 3D point clouds that encode split information from their Kd-trees in the following way: every split on every level is one-hot encoded and concatenated to resulting feature vector. We then use a linear classifier on such a representation (which is also shown as red/blue bars in Figure 2). This baseline evaluates how much information can be recovered from the split orientation information with very little effort.

We also evaluate a model ablation corresponding to our full method with the exception that we remove the the first source information. To this end, we make each leaf representation equal a one-dimensional vector (i.e. scalar) that equals one, effectively removing the first source of information.

The results in Table 2 suggest shows that the first (linear classification) baseline performs much worse than Kd-network (even without leaf information), which suggests that multi-stage hierarchical data flow and intricate weight sharing mechanism of Kd-networks plays an important role (note, however that this baseline performs considerably better than chance suggesting that the orientation of splits in a kd-tree can serve as shape descriptor). Most interestingly, the ablated version of Kd-network comes very close to the full method, highlighting that the second source of information (split direction) dominates the first in terms of importance (confirming the suitability of kd-trees for shape description).

Finally, in Table 2 we assess the importance of two different augmentations as well as the relative performance of randomized and deterministic trees. These experiments suggest that the randomization of Kd-tree boosts the performance (generalization) considerably, while the geometric augmentations give a smaller effect.

Kd-tree depth experiments. For better understanding

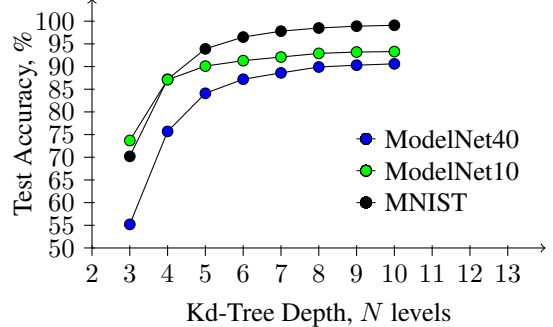


Figure 4. **Kd-tree depth experiments.** Test accuracy for *Kd-networks* learned on clouds of different size 2^N (corresponding to Kd-tree depth N). Saturation without overfitting can be observed.

of the effect of depth, we also conducted a series of experiments corresponding to trees of different depths (Figure 4) of less or equal than ten. To obtain Kd-network architectures for smaller depths we simply remove initial layers from our 10-depth architecture (described above).

Apart from the saturating performance, we observe that the learning time for each epoch for smaller models becomes very short but the number of epochs to achieve convergence increases. For bigger models the time of Kd-tree construction (and point sampling) becomes the bottleneck in our unoptimized implementation.

4.2. Shape retrieval

Dataset and data processing. For the purpose of evaluation for 3D shape retrieval task we use ShapeNetCore dataset [7]. ShapeNetCore is a subset of full ShapeNet dataset of 3D shapes with manually verified category annotations and alignment. It consists of 51300 unique 3D shapes divided into 55 categories each represented by its triangular meshes. For our experiments we used a distribution of the dataset and a training/validation/test split provided by the organizers of 3D Shape Retrieval Contest 2016 (SHREC’16) [26]. Apart from the aligned shapes this distribution contains a perturbed version of the dataset, which consists of the same shapes each perturbed by a random rotation. Also, there is an additional division into several sub-categories available for each category. In our experiments we evaluate on both versions of the dataset. Point clouds for further computations were obtained in the fashion similar to the case of ModelNet datasets.

Training and test procedures. We used a two stage training procedure for the object retrieval task. Firstly, the network was trained to perform classification task in the manner described above. Secondly, the final layer of the network predicting the class posterior was removed, resulting representations of point clouds were normalized and used as shape descriptors provided for the fine-tuning of the network with histogram loss. A mini-batch of size 110 was

	Micro					Macro				
	P@N	R@N	F1@N	mAP	NDCG@N	P@N	R@N	F1@N	mAP	NDCG@N
Tatsuma [26]	0.427	0.689	0.472	0.728	0.875	0.154	0.730	0.203	0.596	0.806
Wang [26]	0.718	0.350	0.391	0.823	0.886	0.313	0.536	0.286	0.661	0.820
Li [26]	0.508	0.868	0.582	0.829	0.904	0.147	0.813	0.201	0.711	0.846
Bai [26]	0.706	0.695	0.689	0.825	0.896	0.444	0.531	0.454	0.740	0.850
Su [26]	0.770	0.770	0.764	0.873	0.899	0.571	0.625	0.575	0.817	0.880
Kd-network	0.760	0.768	0.743	0.850	0.905	0.492	0.676	0.519	0.746	0.864

Table 3. **Retrieval results on normal version of ShapeNetCore dataset** for the metrics introduced in [26] (higher is better). See [26] for the details of metric and the presented systems (in general, all systems in [26] incorporated some variants of 2D multi-view ConvNets). Kd-networks perform on par with the system of Su et al. that is based on multi-view ConvNet[30] and generally better than other methods.

	Micro					Macro				
	P@N	R@N	F1@N	mAP	NDCG@N	P@N	R@N	F1@N	mAP	NDCG@N
Tatsuma [26]	0.372	0.622	0.413	0.638	0.838	0.126	0.657	0.166	0.496	0.743
Wang [26]	0.486	0.212	0.246	0.600	0.776	0.187	0.319	0.163	0.478	0.695
Li [26]	0.467	0.789	0.534	0.749	0.865	0.134	0.714	0.182	0.579	0.767
Bai [26]	0.678	0.667	0.661	0.811	0.889	0.414	0.496	0.423	0.730	0.843
Su [26]	0.632	0.613	0.612	0.734	0.843	0.405	0.484	0.416	0.662	0.793
Kd-network	0.473	0.519	0.451	0.617	0.814	0.205	0.529	0.241	0.484	0.726

Table 4. **Retrieval results on perturbed version of ShapeNetCore dataset**, for the metrics introduced in [26] (higher is better). For the perturbed version of the dataset, Kd-network comes “in the middle of the pack”. This degradation in performance reflects the fact that Kd-network representation is sensitive to global rotation.

used for training, each containing two randomly selected shapes from each category of the dataset. Both training and predicting was done with geometric perturbations and Kd-tree randomization applied. The parameters of the augmentations were taken from the classification task. To improve stability and quality of prediction at test time for each model the descriptors were averaged over several (16 in this experiment) randomized Kd-trees before normalization.

Benchmarking retrieval performance. We compare our results (Table 3 and Table 4) with the results of the participants of SHREC’16 for both normal and perturbed versions of ShapeNetCore. All participating teams of SHREC’16 challenge used systems based on multi-view 2D ConvNets. We use the metrics introduced in [26]. Macro averaged metrics are computed by simple averaging of a metric across all shape categories, micro averaged metrics are computed by weighted averaging with weights proportionate to the number of shapes in a category. A depth-15 Kd-network trained with the histogram loss [32] was used for this task with leaf representation of size 16 (obtained from the three coordinates using an additional multiplicative layer) and intermediate representations of sizes 32 – 32 – 64 – 64 – 128 – 128 – 256 – 256 – 512 – 512 – 1024 – 1024 – 2048 – 2048 – 512. The obtained descriptors of size 512 were used to compute similarity and make predictions for each shape. A similarity cutoff was chosen from the results obtained on the validation part of the datasets.

In general our method performs on par with the sys-

tem based on multiview CNNs [30], and better than other systems that participated in SHREC’16 for the ‘normal’ set. For the ‘perturbed’ version, the relative performance is worse, which reflects the sensitivity of Kd-networks to global rotations. It is likely that even a simplest heuristics for rotational alignment would boost the performance of Kd-network in this version of the the competition.

4.3. Part Segmentation

Finally, we used the architecture discussed in Section 3.2 to predict part labels for individual points within point clouds (e.g. in a plane each point can correspond to plane’s body, wings, tail or engine).

Dataset and data processing. We evaluate our architecture for part segmentation on ShapeNet-part dataset from [36]. It contains 16881 shapes represented as separate point clouds from 16 categories with per point annotation (with 50 parts in total). In this dataset, both the categories and the parts within the categories are highly imbalanced, which poses a challenge to all methods including ours.

Training and test procedures. Since the number of points, representing each model differs in the dataset, we upsample each point cloud to size 4196. Apart from making data feasible for our method, such upsampling helps with rare classes. The upsampled point clouds then are fed to the architecture shown in the Figure 3, which is optimized with the mean cross entropy over all points in a cloud as a loss function. During test time predictions are computed for the upsampled clouds, then the original cloud is passed through

	mean	aero	bag	cap	car	chair	ear	guitar	knife	lamp	laptop	motor	mug	pistol	rocket	skate	table	board
		plane					phone											
Yi [36]	81.4	81.0	78.4	77.7	75.7	87.6	61.9	92.0	85.4	82.5	95.7	70.6	91.9	85.9	53.1	69.8	75.3	
3DCNN	79.4	75.1	72.8	73.3	70.0	87.2	63.5	88.4	79.6	74.4	93.9	58.7	91.8	76.4	51.2	65.3	77.1	
PointNet [20]	83.7	83.4	78.7	82.5	74.9	89.6	73.0	91.5	85.9	80.8	95.3	65.2	93.0	81.2	57.9	72.8	80.6	
Kd-network	77.2	79.9	71.2	80.9	68.8	88.0	72.4	88.9	86.4	79.8	94.9	55.8	86.5	79.3	50.4	71.1	80.2	

Table 5. **Part segmentation results on ShapeNet-core dataset.** The Intersection-over-Union scores are presented for each category as well as mean IoU are reported. Kd-networks have lower mean IoU than the other methods in the comparison, although for some classes the performance of Kd-networks is competitive or better.

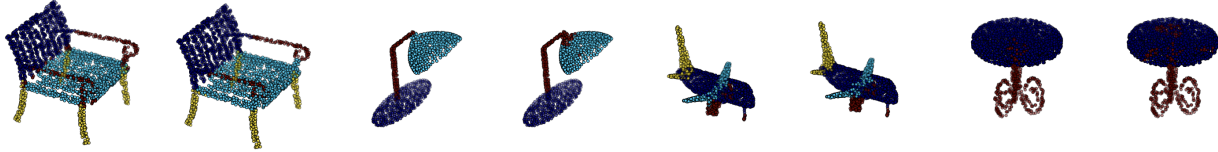


Figure 5. **Examples of part segmentation resulting point labeling.** (use zoom-in for better viewing). Each pair of shapes contain ground truth labeling on the left and predicted labeling on the right. The examples were randomly taken from the validation part of the ShapeNet-core dataset. More results are available in the supplementary material.

a constructed kd-tree to obtain a mapping of each leaf index to corresponding set of original points. This is further used to produce final predictions for every point. Similar to other tasks, we have used data augmentations both during training and test times and averaged predictions over multiple kd-trees.

Benchmarking part segmentation performance. Our results are compared to 3D-CNN (reproduced from [20]), PointNet architecture [20], and the architecture of [36]. For each category mean intersection over union (IoU) is considered as a metric: for each shape IoUs are computed as an average of IoUs for each part which is possible to occur in this shape’s category. Resulting shape IoUs are averaged over all the shapes in the category. A depth 12 variant of Kd-network was used for this task with leaf representations of size 128 and intermediate representations of sizes 128 – 128 – 128 – 256 – 256 – 256 – 512 – 512 – 512 – 512 – 1024. The output of segmentation network is further processed by two fully connected layers of size 512 before the probabilities of the 50 parts present in all classes in the dataset are predicted (the probabilities of the parts that are not possible for a given class are ignored following the protocol of [20]). Batch-normalization is applied to each layer of the whole architecture, and dropout is applied to the final fully connected layers.

In this application, Kd-networks performed worse than the three methods in the comparison in terms of accuracy, which is interesting given that Kd-network outperformed the classification version of the best of the three methods (PointNet [20]) in the ModelNet40 comparison. We speculate that one of the reasons could be insufficient propagation of information across splits withing Kd-tree, although

resulting segmentations do not usually show the signs of underlying Kd-tree structure (Figure 5). Still, the performance of Kd-network for this task does not lag behind other methods significantly. Importantly, the memory footprint of one example during learning is less than 120 Mb (we can fit 35 into a 4Gb memory of our GPU). This footprint is much smaller than for most other deep 3D model segmentation architectures.

5. Conclusion

In this work we propose new deep learning architecture capable of production of representations suitable for different 3D data recognition tasks which works directly with point clouds. Our architecture has many similarities with convolutional networks, however it uses kd-tree rather than uniform grids to build the computational graphs and to share learnable parameters. With our models we achieve results comparable to current state-of-the-art for the variety of recognition problems. Compared to the top-performing convolutional architectures, Kd-trees are also efficient at test-time and train-time.

The competitive performance of our deep architecture based on Kd-trees suggests that other hierarchical 3D space partition structures, such as octrees, PCA-trees, bounding volume hierarchies could be investigated as underlying structures for deep architectures.

References

- [1] J. L. Bentley. Multidimensional binary search trees used for associative searching. *Communications of the ACM*, 18(9):509–517, 1975.

[2] D. Boscaini, J. Masci, S. Melzi, M. M. Bronstein, U. Castellani, and P. Vandergheynst. Learning class-specific descriptors for deformable shapes using localized spectral convolutional networks. *Comput. Graph. Forum*, 34(5):13–23, 2015.

[3] D. Boscaini, J. Masci, E. Rodolà, and M. M. Bronstein. Learning shape correspondence with anisotropic convolutional neural networks. In *Proc. NIPS*, pages 3189–3197, 2016.

[4] A. Brock, T. Lim, J. Ritchie, and N. Weston. Generative and discriminative voxel modeling with convolutional neural networks. *arXiv preprint arXiv:1608.04236*, 2016.

[5] J. Bromley, J. W. Bentz, L. Bottou, I. Guyon, Y. LeCun, C. Moore, E. Säckinger, and R. Shah. Signature verification using a siamese time delay neural network. *International Journal of Pattern Recognition and Artificial Intelligence*, 7(04):669–688, 1993.

[6] J. Bruna, W. Zaremba, A. Szlam, and Y. LeCun. Spectral networks and locally connected networks on graphs. *arXiv preprint arXiv:1312.6203*, 2013.

[7] A. X. Chang, T. Funkhouser, L. Guibas, P. Hanrahan, Q. Huang, Z. Li, S. Savarese, M. Savva, S. Song, H. Su, et al. Shapenet: An information-rich 3d model repository. *arXiv preprint arXiv:1512.03012*, 2015.

[8] S. Chopra, R. Hadsell, and Y. LeCun. Learning a similarity metric discriminatively, with application to face verification. In *Proc. CVPR*, pages 539–546, 2005.

[9] S. Dieleman, J. Schlter, C. Raffel, E. Olson, et al. Lasagne: First release., Aug. 2015.

[10] J. D. Foley, A. Van Dam, S. K. Feiner, J. F. Hughes, and R. L. Phillips. *Introduction to computer graphics*, volume 55. Addison-Wesley Reading, 1994.

[11] A. Guttman. *R-trees: a dynamic index structure for spatial searching*, volume 14. ACM, 1984.

[12] V. Hegde and R. Zadeh. Fusionnet: 3d object classification using multiple data representations. *arXiv preprint arXiv:1607.05695*, 2016.

[13] M. Jaderberg, K. Simonyan, A. Zisserman, and K. Kavukcuoglu. Spatial transformer networks. In *Proc. NIPS*, pages 2017–2025, 2015.

[14] D. Laptev, N. Savinov, J. M. Buhmann, and M. Pollefeys. TI-POOLING: transformation-invariant pooling for feature learning in convolutional neural networks. In *Proc. CVPR*, pages 289–297, 2016.

[15] Y. LeCun, L. Bottou, Y. Bengio, and P. Haffner. Gradient-based learning applied to document recognition. *Proceedings of the IEEE*, 86(11):2278–2324, 1998.

[16] Y. Li, S. Pirk, H. Su, C. R. Qi, and L. J. Guibas. Fpnn: Field probing neural networks for 3d data. In *Proc. NIPS*, 2016.

[17] J. Long, E. Shelhamer, and T. Darrell. Fully convolutional networks for semantic segmentation. In *Proc. CVPR*, pages 3431–3440, 2015.

[18] D. Maturana and S. Scherer. Voxnet: A 3d convolutional neural network for real-time object recognition. In *Proc. IROS*, pages 922–928. IEEE, 2015.

[19] D. J. Meagher. *Octree encoding: A new technique for the representation, manipulation and display of arbitrary 3-d objects by computer*. Electrical and Systems Engineering Department Rensselaer Polytechnic Institute Image Processing Laboratory, 1980.

[20] C. R. Qi, H. Su, K. Mo, and L. J. Guibas. Pointnet: Deep learning on point sets for 3d classification and segmentation. *arXiv preprint arXiv:1612.00593*, 2016.

[21] C. R. Qi, H. Su, M. Niessner, A. Dai, M. Yan, and L. J. Guibas. Volumetric and multi-view cnns for object classification on 3d data. In *Proc. CVPR*, 2016.

[22] S. Ravanbakhsh, J. Schneider, and B. Počzos. Deep learning with sets and point clouds. *arXiv preprint arXiv:1611.04500*, 2016.

[23] A. A. Requicha and H. B. Voelcker. Constructive solid geometry. 1977.

[24] O. Ronneberger, P. Fischer, and T. Brox. U-net: Convolutional networks for biomedical image segmentation. In *Proc. MICCAI*, pages 234–241. Springer, 2015.

[25] H. Samet. *The design and analysis of spatial data structures*, volume 199. Addison-Wesley Reading, MA, 1990.

[26] M. Savva, F. Yu, H. Su, M. Aono, B. Chen, D. Cohen-Or, W. Deng, H. Su, S. Bai, X. Bai, et al. SHREC16 track large-scale 3d shape retrieval from ShapeNet Core-55. In *Proceedings of the Eurographics Workshop on 3D Object Retrieval*, 2016.

[27] M. Schultz and T. Joachims. Learning a distance metric from relative comparisons. *Advances in neural information processing systems (NIPS)*, page 41, 2004.

[28] R. A. Schumacker, B. Brand, M. G. Gilliland, and W. H. Sharp. Study for applying computer-generated images to visual simulation. Technical report, DTIC Document, 1969.

[29] R. Socher, C. C. Lin, C. Manning, and A. Y. Ng. Parsing natural scenes and natural language with recursive neural networks. In *Proc. ICML*, pages 129–136, 2011.

[30] H. Su, S. Maji, E. Kalogerakis, and E. Learned-Miller. Multi-view convolutional neural networks for 3d shape recognition. In *Proc. ICCV*, pages 945–953, 2015.

[31] Theano Development Team. Theano: A Python framework for fast computation of mathematical expressions. *arXiv e-prints*, abs/1605.02688, May 2016.

[32] E. Ustinova and V. S. Lempitsky. Learning deep embeddings with histogram loss. In *Proc. NIPS*, pages 4170–4178, 2016.

[33] D. Z. Wang and I. Posner. Voting for voting in online point cloud object detection. In *Proc. RSS*, 2015.

[34] J. Wu, C. Zhang, T. Xue, B. Freeman, and J. Tenenbaum. Learning a probabilistic latent space of object shapes via 3d generative-adversarial modeling. In *Proc. NIPS*, pages 82–90, 2016.

[35] Z. Wu, S. Song, A. Khosla, F. Yu, L. Zhang, X. Tang, and J. Xiao. 3d shapenets: A deep representation for volumetric shapes. In *Proc. CVPR*, pages 1912–1920, 2015.

[36] L. Yi, V. G. Kim, D. Ceylan, I. Shen, M. Yan, H. Su, A. Lu, Q. Huang, A. Sheffer, L. Guibas, et al. A scalable active framework for region annotation in 3d shape collections. *ACM Transactions on Graphics (TOG)*, 35(6):210, 2016.

Appendix

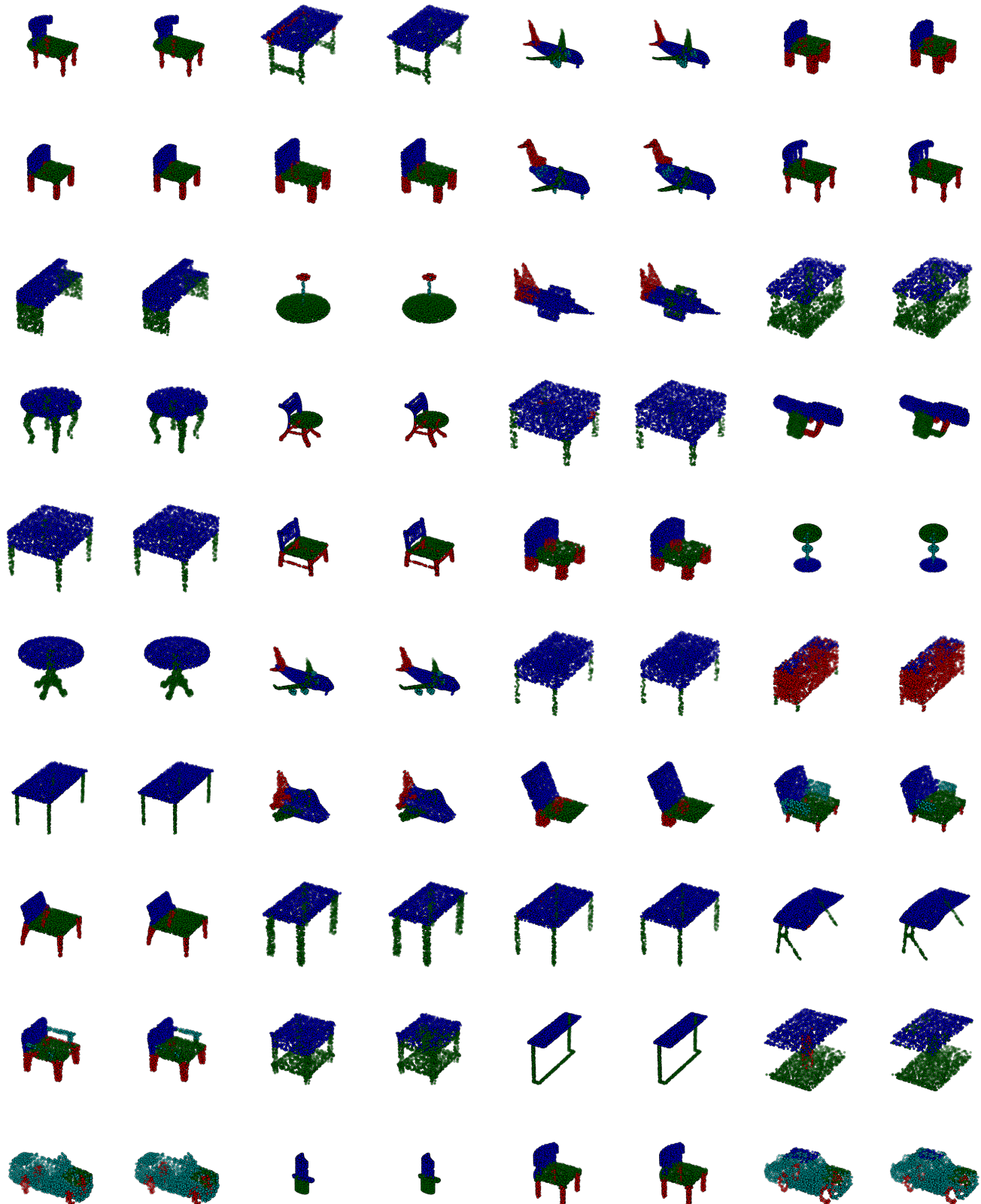


Figure 6. Part segmentation results. (use zoom-in for better viewing). The results for the first 40 point clouds from the test set of the ShapeNet-core part segmentation dataset are shown. In each pair, the ground truth labeling is shown on the left and the labeling predicted by our model is shown on the right. The color coding denotes part labels and is separate for different object classes.

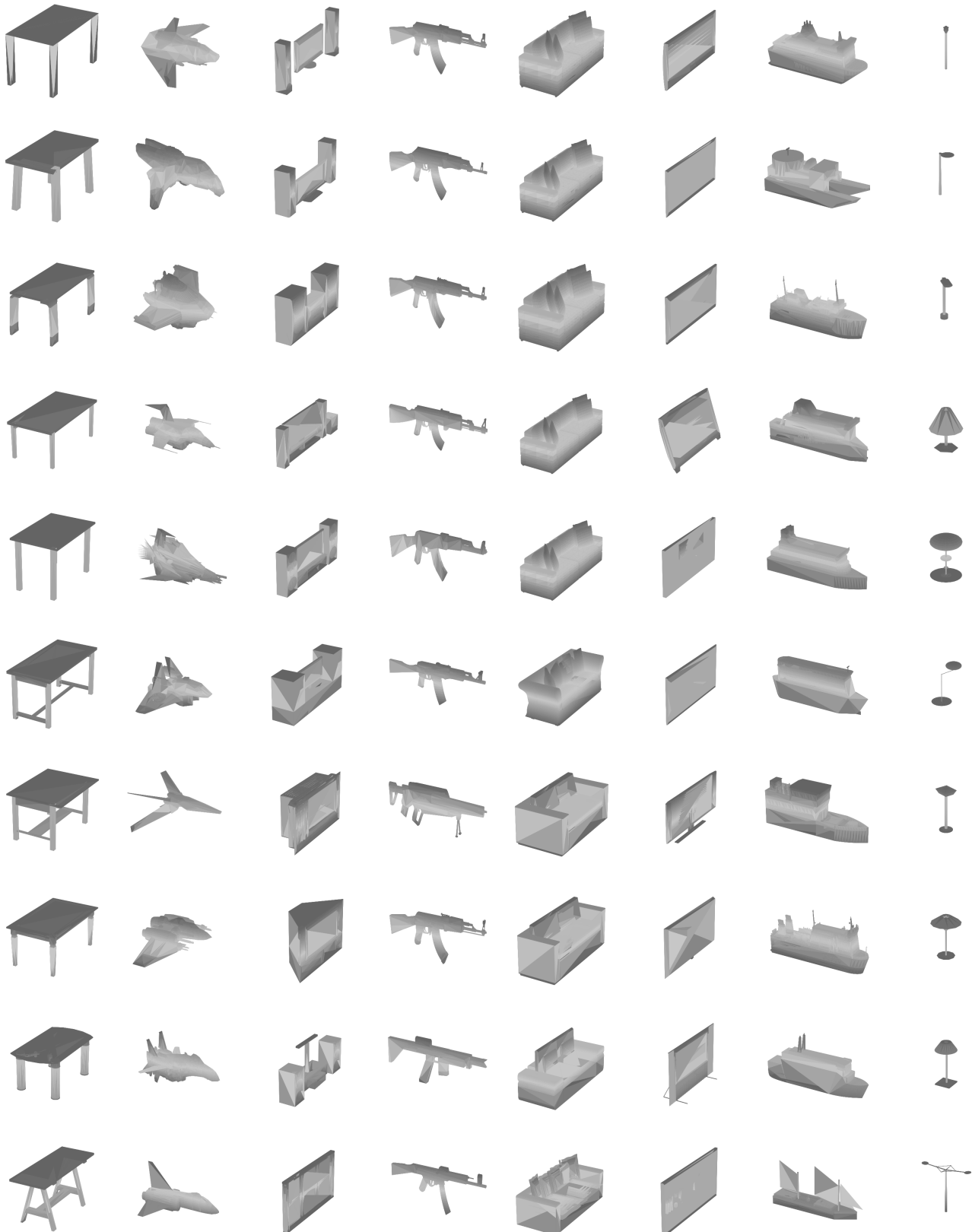


Figure 7. **Shape retrieval results.** First eight query shapes along with nine retrieved shapes from the test part of the normal ShapeNet-core retrieval dataset. Each column shows the query in the top and the retrieved models sorted according to the cosine similarity of Kd-descriptors below.

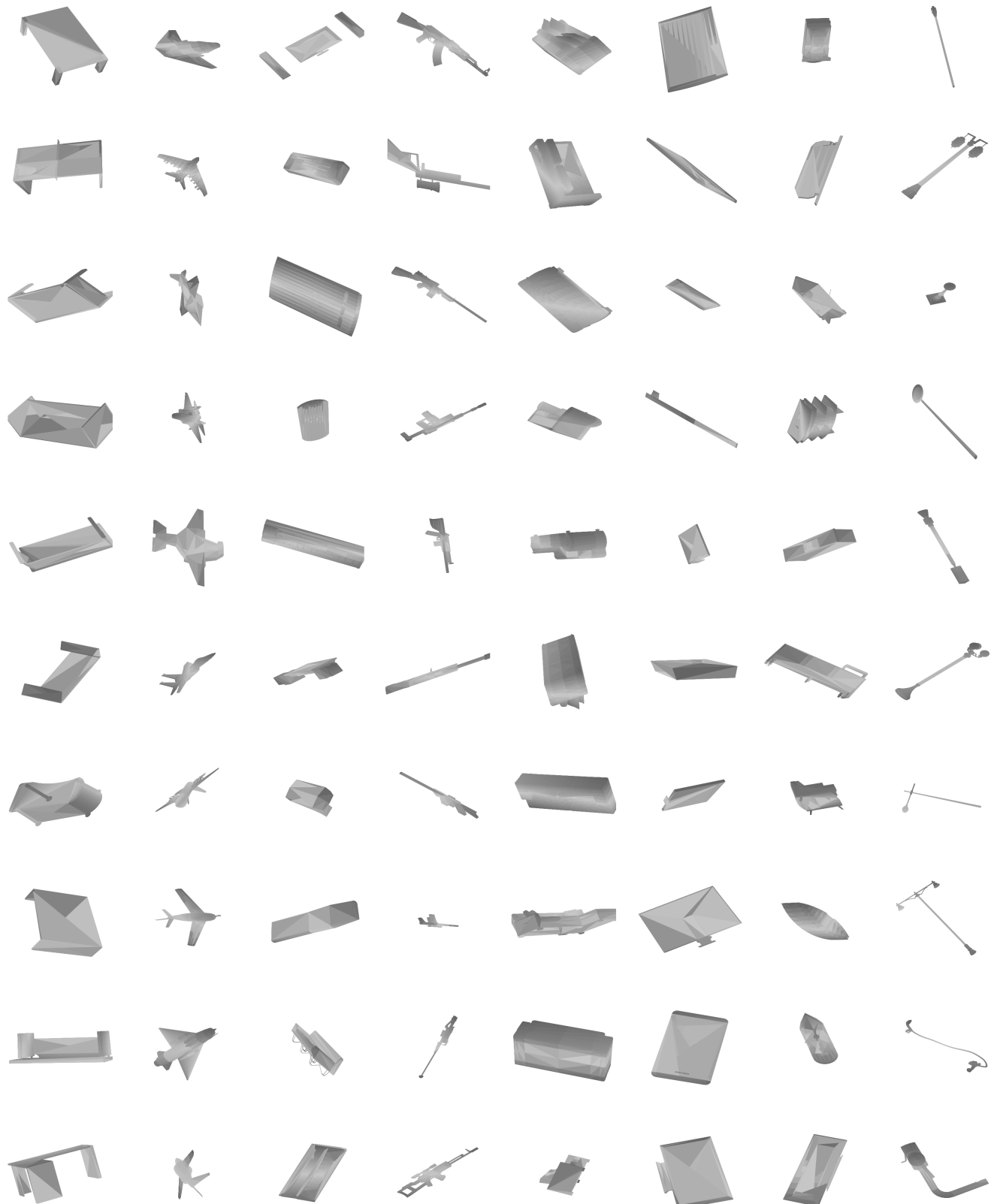


Figure 8. Shape retrieval results. First eight query shapes along with nine retrieved shapes from the test part of the perturbed ShapeNet-core retrieval dataset. Each column shows the query in the top and the retrieved models sorted according to the cosine similarity of Kd-descriptors below.

A. Qualitative results

In the previous pages, we present qualitative results for shape retrieval and shape part segmentation tasks. We show the results for the ShapeNet Part Segmentation dataset (Figure 6) and the ShapeNet Core55 Retrieval dataset (the aligned version in Figure 7, and the perturbed version in Figure 8). The results are given for the first examples in the test sets (no “cherry picking” was applied).